(Received 4 April 2025, Accepted 21 May 2025, Scheduled 29 May 2025)

Low-Profile Reconfigurable UWB Fractal Antenna Enhanced by Parasitic Elements for Wireless Applications

Mohamed Marzouk[1], Ibrahime H. Nejdi[2], Youssef Rhazi[1], Mohamed Saih[1], Jamal A. Nasir[3], Abdulrahman Daher[4], Mousa I. Hussein[4], Zahriladha Zakaria[5], and Ahmed J. A. Al-Gburi[5,*]

[1]*Microelectronics, Embedded Systems and Telecommunications Faculty of Sciences and Technology, Sultan Moulay Slimane University, Beni-Mellal, Morocco*
[2]*Automatic and Energy Conversion, Faculty of Science and Technology Sultan Moulay Slimane University, Beni-Mellal, Morocco*
[3]*Department of Electrical Engineering, Faculty of Engineering & Technology, Gomal University, Pakistan*
[4]*Electrical and Communication Engineering Department, United Arab Emirates University, UAE*
[5]*Center for Telecommunication Research & Innovation (CeTRI) Fakulti Teknologi Dan Kejuruteraan Elektronik Dan Komputer (FTKEK) Universiti Teknikal Malaysia Melaka (UTeM), Jalan Hang Tuah Jaya, Durian Tunggal, Melaka 76100, Malaysia*

ABSTRACT: This paper presents an enhanced design of a reconfigurable fractal ultra-wideband (UWB) antenna, improved through the inclusion of parasitic elements. The antenna incorporates two plus-shaped parasitic elements and a hexagonal radiating patch, while maintaining compact dimensions of 30 mm × 22 mm × 1.6 mm on an FR4 substrate. A partial ground plane with an integrated rectangular slot is etched on the backside of the resonator. The antenna was designed using HFSS, fabricated, and experimentally validated. The measured results show good agreement with the simulations. It operates over a frequency range of 4 to 10.57 GHz, with resonant frequencies at 4.7, 7.92, and 10 GHz. The design achieves a gain between 2.76 and 5.83 dB and maintains high radiation efficiency ranging from 82% to 95%. To further enhance performance, two strategically placed HPND-4005 PIN diodes are incorporated, allowing tunable resonance characteristics by altering current distribution under various switch configurations. As a result, the reconfigurable antenna extends its operational bandwidth from 3 to 14 GHz, making it suitable for a variety of wireless applications such as Wi-Fi, WiMAX, WLAN, and C-, X-, and Ku-band communications. Notably, the design achieves this wideband reconfigurability using only two PIN diodes while maintaining a compact footprint — offering an advantage over previous designs. Its features support seamless integration into compact electronic devices, enabling manufacturers to incorporate multiple antennas with minimal complexity.

1. INTRODUCTION

In an era dominated by wireless communication, antennas are essential components that facilitate the connection between the digital and physical domains [1–4]. From the towering structures of broadcast antennas to the minuscule components inside smartphone, these devices play a pivotal role in ensuring that one stays connected in our interconnected world [5–8].

One of the key features of fractal antennas is their compact size, which is a significant advantage in a world where miniaturization is a constant pursuit [9–15]. By efficiently using space, fractal antennas can be integrated into a variety of devices, from smartphones and wearable technology to military equipment and satellites. However, their true potential is unlocked when parasitic elements are introduced into the antenna.

Parasitic elements are passive components strategically placed near the radiating elements of an antenna. These elements can be manipulated to change the antenna's performance characteristics [16–19]. They serve as the antenna's "adjustment knobs," enabling it to be fine-tuned for specific operating frequencies or scenarios. By adjusting the parasitic elements, the antenna can dynamically switch between different configurations, optimizing its performance based on the demands of the moment. The combination of fractal geometry and parasitic elements opens up a world of possibilities for wireless communication. A single antenna on a mobile device effortlessly switches among Wi-Fi, cellular, and satellite communication, maintaining optimal performance throughout, owing to the integration of parasitic elements. This level of adaptability is precisely what reconfigurable fractal antennas with parasitics promise to deliver. These antennas are not limited to consumer devices; they have wide-ranging applications in the fields of telecommunications [20–24], aerospace, and defense. In satellite communication, for instance, reconfigurable fractal antennas can adapt to various frequency bands, maximizing the efficiency of data transfer between Earth and orbiting spacecraft. In military applications, the ability to switch frequencies and adapt to changing conditions is invaluable. The innovation of reconfigurable fractal antennas with parasitics also has significant implications for the Internet of Things (IoT). As IoT devices continue to proliferate, the need for versatile, space-efficient antennas becomes increasingly crucial. These antennas can be embedded in a multitude of IoT devices, from

* Corresponding author: Ahmed Jamal Abdullah Al-Gburi (ahmedjamal@ieee.org, ahmedjamal@utem.edu.my).

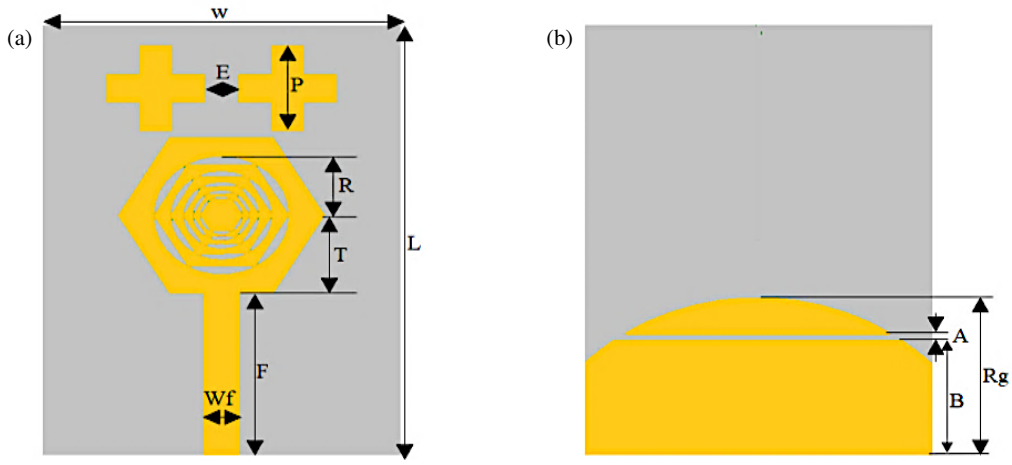

FIGURE 1. (a) Frontal plane view of the antenna design; (b) Ground plane configuration of the antenna proposal.

smart home sensors to industrial equipment, ensuring reliable connectivity in a diverse range of environments. Beyond the technical advantages, the development of reconfigurable fractal antennas with parasitics aligns with the broader goals of sustainability and resource efficiency. Their ability to operate across multiple frequencies can lead to a reduction in the number of antennas required for various applications, minimizing the environmental impact associated with manufacturing and deployment.

In the constantly evolving field of wireless communication, the growing need for faster data transfer rates, pinpoint location tracking, and efficient short-range communication has catalyzed the emergence of groundbreaking technologies. Leading this charge is ultra-wideband (UWB) antenna [25–27], a new technology leading the way in innovation. Diverging from traditional counterparts, UWB antennas exhibit an exceptional capacity to operate seamlessly across an extensive frequency spectrum, ranging from several hundred megahertz to several gigahertz [28–30]. This distinctive attribute not only facilitates rapid data transfer but also opens a gateway to a plethora of applications, spanning from high-speed data communication to precision location sensing [31, 32]. The article [33] presents a cedar-shaped coplanar waveguide-fed frequency-reconfigurable antenna designed for wireless communication. Using low-cost materials, it incorporates PIN diodes to manipulate current distribution and adjust resonant frequencies. Tested from 2.5 GHz to 10 GHz, it covers aviation service, WLAN, WiMAX, radio telecommunications, and satellite communication. In [34], the paper emphasizes the crucial role of corrosion resistance in ensuring the reliability of reconfigurable filtering antenna, particularly in the realm of UWB applications. Conventional corrosion prevention methods prove inadequate due to the limited intrinsic corrosion resistance of metal-based devices. The study introduces a corrosion-resistant reconfigurable filtering antenna utilizing a graphene-assembled film (GAF), showcasing electrical performance comparable to copper-based antennae. Notably, the GAF-based antenna displays versatility in transitioning between UWB (2.8–11 GHz) and narrowband filtering (NBF, 3.23–3.77 GHz) modes, indicating promising prospects for communication systems in challenging environments.

The researchers in this study successfully manufactured a fractal antenna integrated with parasitic elements and a partial ground plane, known for its wide-ranging performance. This achievement was made possible by combining fractal slots with an FR-4 substrate as structural support. Remarkably compact, with dimensions of 30 mm $\times$ 22 mm $\times$ 1.6 mm, this innovative model exhibits excellent radiation characteristics. It is highly versatile and well suited for various wireless communication technologies, operating within the 4–10.57 GHz frequency range. These applications include popular standards such as Wi-Fi, Bluetooth, WiMAX, WLAN, and C- and X-band communications.

To further enhance the antenna's electrical characteristics, two strategically positioned PIN diodes are integrated. These diodes play a crucial role in modulating current distribution and adjusting resonant frequencies through different switch configurations. As a result, the reconfigurable antenna extends its resonance capability to cover the ultra-wideband (UWB) frequency range of 3–14 GHz.

2. DESIGN CONFIGURATION FOR THE PROPOSED FRACTAL ANTENNA

Figure 1 shows the geometry of the wide-band antenna suggested in this study. The design is meticulously crafted, comprising four essential components — the patch, feed line, partial ground plane, and parasitic elements. Notably, parasitic patch elements strategically positioned at the top of the antenna contribute to improved impedance adaptation.

After conducting simulations, it was found that placing the parasitic elements at the top of the antenna yielded the best results, leading to an expanded reflection coefficient S_{11}, increased peak gain, and a reduction in the overall size of the antenna. Experimental results validate these findings, indicating increased efficiency. Overall, the literature supports that parasitic elements effectively enhance gain and radiation patterns, confirming their crucial role in superior impedance adaptation.

TABLE 1. Details of the suggested antenna.

Parameters	L	W	F	T	R	Wf	P	E	A	Rg	B
Values (mm)	30	22	11	6	3.75	2.25	6	2	0.5	11	8

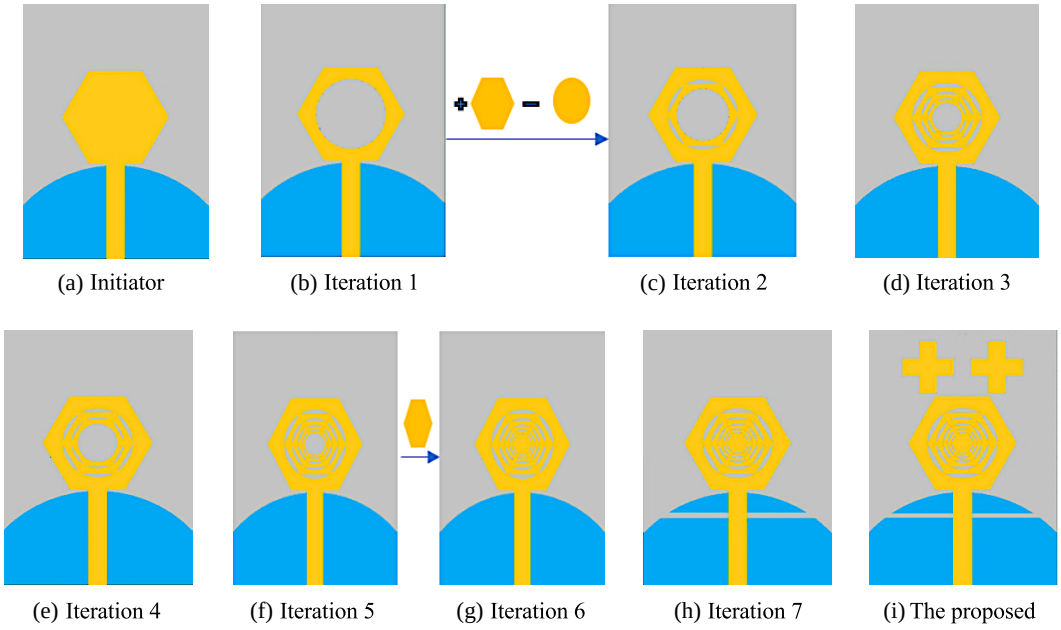

(a) Initiator (b) Iteration 1 (c) Iteration 2 (d) Iteration 3

(e) Iteration 4 (f) Iteration 5 (g) Iteration 6 (h) Iteration 7 (i) The proposed

FIGURE 2. Phases adopted to attain the ideal design for the proposed antenna.

The antenna itself features a modified hexagonal radiator, simply printed on a cost-effective FR4 substrate. On the opposing side of the substrate, a partial ground plane is incorporated, distinguished by an integrated rectangular slot with a thickness of $A = 0.5$ mm, enhancing the overall performance. Incorporating a partial ground plane with an integrated rectangular slot of a thickness of $A = 0.5$ mm, significantly enhances antenna performance. The ground plane improves gain while the rectangular slot introduces additional resonant modes, resulting in broader bandwidth and better impedance matching. As seen in simulations, these modifications lead to increased bandwidth and improved gain and radiation patterns. Additionally, the slot acts as an extra radiating element, enhancing coupling with the feed line and overall efficiency. Existing literature supports these benefits, demonstrating the effectiveness of this design modification. The dielectric substrate chosen for this antenna design has a thickness of 1.6 mm, ensuring optimal functionality. In this work, a microstrip feed line of impedance 50 Ω is adopted, further contributing to the antenna's efficiency. The meticulous optimization of the antenna was conducted using the High-Frequency Structure Simulator (HFSS). The specific dimensions of the proposed antenna are detailed in Table 1, providing comprehensive insights into its size and proportions. With a compact form factor of 30 mm × 22 mm, this antenna stands as a testament to the fusion of precision engineering and advanced optimization techniques, promising superior wideband performance.

In this study, the utilization of fractal geometry is integral to enhancing the performance of a patch antenna. The fractal geometry relies on a hexagonal structure that repeats itself with a reduction factor of 3/4. The antenna evolution process commenced with a basic hexagonal shape as the initial configuration (refer to Fig. 2(a)), which included a circular partial ground. To identify the resonant frequency of a hexagonal patch antenna, (1), which pertains to a circular strip patch antenna and is documented in [35] and [36], was employed.

$$f_r = \frac{y_{mn}c}{5.714R_e\sqrt{\varepsilon_{reff}}} \tag{1}$$

In the context where c represents the speed of light in free space, and ε_{reff} is the effective dielectric constant, for the TM_{11} mode, y_{mn} takes the specific value of $y_{11} = 1.8412$. Furthermore, the effective radius (R_e) of the circular patch antenna is determined using (2).

$$R_e = R_c\sqrt{1 + \frac{2h}{R_c\pi\varepsilon_r}\left(\ln\left(\frac{\pi R_c}{2h}\right) + 1.7726\right)} \tag{2}$$

R_c signifies the radius of the circular patch antenna.

By establishing equivalence in the areas of circular and hexagonal patch antennas, one can employ the resonant frequency for the purpose of hexagonal patch antenna design

$$\pi R_e^2 = \frac{3}{2}\sqrt{3}S^2 \tag{3}$$

where S represents the side length of the hexagonal patch antenna.

The initiator design of the suggested antenna employed a fundamental hexagonal patch, operating at a frequency [4.55–6.34] GHz. The side length (S) of the conventional hexagonal patch antenna was calculated to be 9 mm using (1) through (3). The exact resonant frequency of the hexagonal patch antenna can be determined through simulation, where the f_r parameter is analyzed. Fig. 3 demonstrates the antenna's performance through different iterations of the design. By examining the f_r results from these simulations, it is possible to identify the frequency at which the antenna achieves optimal performance, thus pinpointing the exact resonant frequency within the specified range of [4.55–6.34] GHz. This process allows for a clear understanding of how design changes impact the resonant characteristics of the antenna.

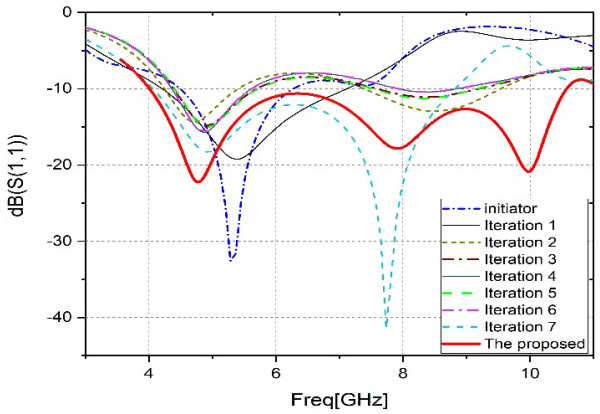

FIGURE 3. S_{11} parameter evaluation across different design phases.

Subsequent iterations aim to refine and broaden the antenna's frequency response. In the first iteration (Fig. 2(b)), a hexagonal shape where a disk is cut inside it has been added to the resonator, extending the frequency range to [4.14–7.8] GHz. To further optimize matching, a third circle-inscribed hexagon is incorporated into the radiator in iteration 2 design (Fig. 2(c)), resulting in a new frequency band of [4.28–5.36] and [7.34–9.55]. Successive iterations 3, 4, and 5 (Figs. 2(d), (e), and (f)) involve the addition of circle-inscribed hexagonal radiators, strategically chosen to achieve a wide band response within the target frequency range.

In the sixth iteration in Fig. 2(g), a single hexagonal radiator is centrally added to the patch, providing a broad frequency band of [4.14–7.16] GHz. The seventh iteration in Fig. 2(h) introduces a modification to the ground, incorporating a rectangular slot with a 0.5 mm thickness. This modification leads to a considerably broader bandwidth of 4.9 GHz.

Furthermore, in the proposed antenna, the inclusion of parasitic patch elements, in the form of two plus-shaped structures attached to the antenna's top, serves as an additional technique to enhance performance as seen in Fig. 2(i). These parasitic elements are strategically designed to broaden the bandwidth of the patch antenna by an impressive 6.57 GHz.

The entire design process involves a thoughtful combination of fractal geometry, iterative adjustments to the patch structure, and the incorporation of parasitic elements. The simulation results and optimization processes undertaken throughout these iterations are aimed at achieving specific performance parameters for the antenna, ultimately producing a wideband response within the target frequency range.

This patch exhibits compatibility with a diverse range of wireless communication technologies, including Wi-Fi, WLAN, WiMAX, and Radar Systems, spanning the C and X bands. The frequency spectrum covered by this patch ranges from 4 GHz to 10.57 GHz, encompassing a portion of the IEEE-defined C-band and aligning with the broader X-band. Although the antenna's coverage does not extend across the entire X-band spectrum, it is adept at supporting numerous applications within these specified frequency ranges. Fig. 3 illustrates the S_{11} parameter across various stages of the design. It offers a visual representation of how the S_{11} values evolve as the design progresses, providing valuable insights into the antenna's performance characteristics throughout its development.

3. RESULTS AND DISCUSSION

To demonstrate the exceptional performance of the suggested antenna design, this section presents both simulation and measurement results. An essential element of this design is the use of an FR4 substrate with optimal dimensions of 30 mm $\times$ 22 mm $\times$ 1.6 mm, which is used to fabricate the proposed fractal antenna. The antenna size is specified in terms of the lowest resonating frequency as $0.166\lambda \times 0.226\lambda \times 0.012\lambda$.

To assess the antenna's performance, a vector network analyzer was employed to measure its reflection coefficient. In Fig. 4, the physical prototype of the hexagon-shaped fractal antenna is depicted, showcasing its front Fig. 4(a), back Fig. 4(b) views, and its placement inside the chamber Fig. 4(c). In Fig. 5, a comparison between the reflection coefficient responses obtained through experimentation and simulation is provided. Notably, these results exhibit a remarkable level of agreement. Some disparities exist between the measured and simulated outcomes. These disparities can be attributed to various factors, including environmental conditions, the effects of SMA soldering, substrate quality, and fabrication process inaccuracies.

To assess the proposed wideband antenna's reflection coefficient, we utilized a Vector Network Analyzer (VNA). The results show a close match between the simulated and measured reflection coefficients, affirming the antenna's wideband functionality across a diverse frequency spectrum as shown in Fig. 5. Nevertheless, a slight variance was noted, likely attributed to manufacturing and measurement conditions. The discrepancy between the simulated and measured results of the FR4 patch antenna, as illustrated in Fig. 5, can be largely attributed to substrate instability, which causes significant variations in dielectric properties and leads to performance mismatches. Additionally, fabrication tolerances can introduce dimensional variations, while environmental conditions during measurement may not align with the assumptions made in the simulations. Variations in the feeding mechanism or impedance matching may also contribute to the observed differences.

The recommended antenna boasts a broad frequency range of 6.5 GHz, encompassing frequencies from 4 GHz

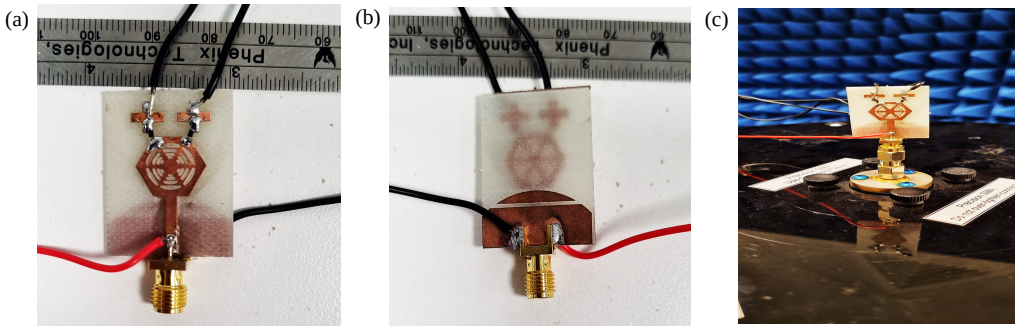

FIGURE 4. Antenna fabrication: (a) upper and (b) lower views of the manufactured antenna, with (c) the antenna placed inside an anechoic chamber.

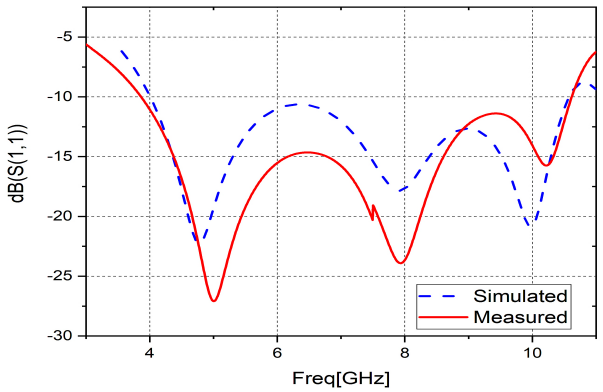

FIGURE 5. Comparison of simulated and measured S_{11} reflection coefficients.

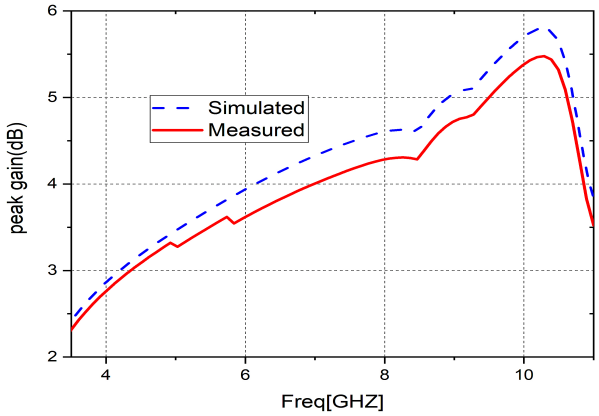

FIGURE 6. Comparison of simulated and measured peak gains.

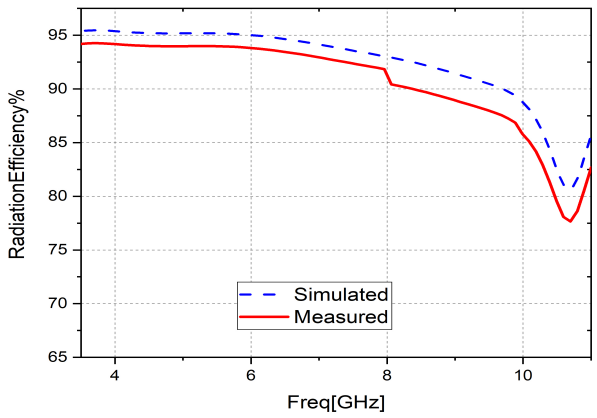

FIGURE 7. Comparison of simulated and measured radiation efficiencies.

to 10.57 GHz, with resonant frequencies identified at 4.7, 7.9, and 10 GHz. This design facilitates wide coverage, including WiFi/WLAN (5.2 GHz (5.15–5.35 GHz)/5.8 GHz (5.725–5.825 GHz)), 3.5 GHz (3.3–3.8 GHz), 5.5 GHz (5.25–5.85 GHz), and (5.25–5.85 GHz) for (WiMAX), C band (4 to 8) GHz, and X band (8 to 12) GHz.

Anechoic chamber serves as a meticulously controlled environment, eliminating external noise and interference. This controlled setting enables precise measurements of the antenna's radiation pattern, gain, and efficiency. Utilizing an anechoic chamber ensures that measurements remain unaffected by reflections from nearby objects, ground, or other structures, preventing distortions in the results. In Fig. 6, the peak gains graph illustrates a close alignment between the simulated and measured values. This alignment reinforces the reliability of the measurements. According to the data, the proposed antenna demonstrates peak realized gains ranging from 2.78 dB to 5.83 dB.

The notable simulated radiation efficiency of 95% highlights the effective energy radiation capability of the suggested antenna across various frequencies within its operating band. The measured radiation efficiency, ranging from 82% to 95% across the band, solidifies the antenna's efficiency in transmitting or receiving signals across the entire frequency spectrum.

The drop in gain and radiation efficiency near 10 GHz is mainly due to the increased dielectric losses of the FR4 substrate at high frequencies. As frequency rises, FR4 absorbs more electromagnetic energy, which reduces radiation efficiency and degrades overall antenna performance.

Figure 7 presents a visual representation of these radiation efficiency values, offering crucial insights into the antenna's performance. The consistently high radiation efficiency observed throughout the operating band positions the antenna as a compelling choice for diverse applications requiring efficient signal transmission or reception at varying frequencies.

Figure 8 presents the simulated and measured two-dimensional radiation attributes of the recommended fractal antenna. The analysis is performed on the YZ and XZ planes at three distinct frequencies: 4.76 GHz, 7.92 GHz, and 10 GHz. Observations in the figure indicate that the designed antenna displays bidirectional radiation characteristics in the YZ

TABLE 2. Performance comparison between the proposed antenna and reference designs from existing literature.

Ref.	Size (mm^3)	Type of Substrate	Bandwidth (GHz)	Resonant Frequency (GHz)	Peak Gain dB	Efficiency %	Antenna Design
[9]	$40 \times 40 \times 1.6$	FR4	3.86–3.94 5.96–7.38 8.2–8.9	3.8 5.66 8.3	-	-	Sierpinski carpet fractal antenna
[10]	$40 \times 35 \times 1.6$	FR4	5–10	5.16, 6.6, 7.211, 8.32, 9.96	-	-	Slot-based triangular patch fractal antenna
[11]	$38 \times 38 \times 2.4$	FR4	3.50–3.56 6.58–6.61 8.4–8.52	3.53 6.54 8.48	6	-	I shape fractal antenna
[12]	$60 \times 55 \times 1.59$	FR4	4.30–4.37 4.95–5.1 6.17–6.32 7.48–7.50 9.21–9.24	4.31, 5.05, 6.30, 7.49, 9.23	1.08–4.87	-	Fractal Koch antenna
[13]	$16 \times 16 \times 0.8$	FR4	7.16–8 11.5–12.39	7.6 12	-	-	Pentagonal-shaped fractal antenna
[14]	$24 \times 36 \times 1.6$	FR4	3.3–6.0	3.5, 4, 4.5, 5.5	-	95	Slot fractal antenna
[16]	$35 \times 35 \times *$	ECCOSTOCK HIK	3.30–4.38	3.9	-	-	Parasitic patch
[17]	$25 \times 34.5 \times 1.575$	Rogers RT 5880	2.75–4.23	3.14	2.22 to 2.77	92	Slotted Parasitic
[18]	$30 \times 32 \times 1.6$	FR4	3.8–9	5.8 8.2	-	-	U-shaped radiator and parasitic strip
[19]	$40 \times 70 \times 1.6$	FR4	4.89–6.85	5.3 6.5	6.5	87	Square parasitic elements
[20]	$22 \times 22 \times 1.6$	FR4	3.3–7.1	3.5, 4.5, 5.5, 6.5	4.6-6.2	48–89	MIMO antenna arrays
[21]	$15 \times 30 \times 1$	FR4	4.1–6	4.5 5	-	-	Fractal MIMO antenna
The Proposed	$30 \times 22 \times 1.6$	FR4	4 to 10.57	4.76, 7.92, 10	2.76 to 5.83	82 to 95	Parasitic patch

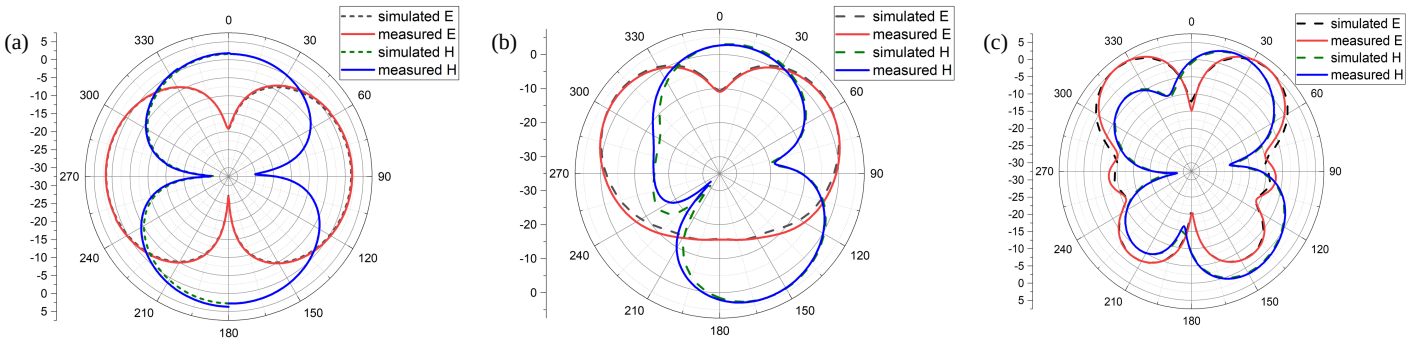

FIGURE 8. Radiation patterns of the hexagonal fractal antenna at selected frequencies at (a) 4.76 GHz, (b) 7.92 GHz, and (c) 10 GHz: a comparison of simulated and experimental results.

plane and omnidirectional properties in the XZ plane. These valuable characteristics enable the recommended antenna to be a strong option for several applications.

Table 2 presents a comparison between the recommended antenna and others found in existing literature, focusing on Size, Type of Substrate, Bandwidth, Resonant Frequency, Peak Gain, Efficiency, and Antenna Design. The proposed slot-based triangular patch fractal antenna, as suggested by [10], operates within the 5 to 10 GHz bandwidth, with dimensions of 40 mm × 35 mm and resonates at frequencies 5.16, 6.6, 7.211, 8.32, and 9.96 GHz. In contrast, [13] introduces a dual-band antenna with a size slightly smaller and operating from 7.16 to

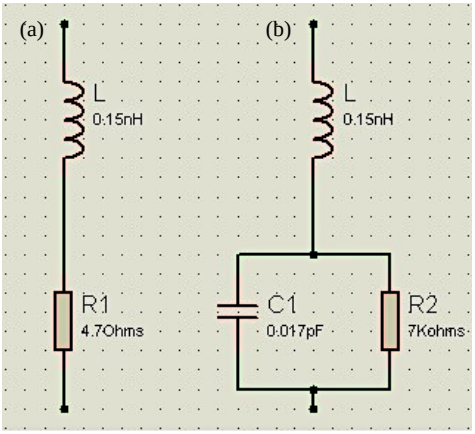

FIGURE 9. Modeling the circuit equivalents for (a) ON state; (b) OFF state.

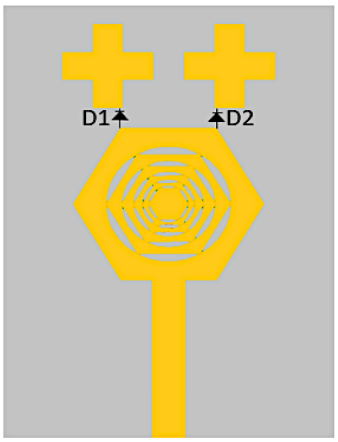

FIGURE 10. Diodes placement in antenna configuration.

8 GHz and 11.5 to 12.39 GHz on an FR4 substrate. The antenna in [14], designed for wireless computer networks like Wi-Fi and C-band, boasts a bandwidth from 3.3 to 6 GHz and an efficiency exceeding 92%. Conversely, the antenna in [16] has a larger size of 35 mm × 35 mm and operates in a narrow band with an ECCOSTOCK HIK substrate. Ref. [19] presents a patch with dimensions of 40 mm × 70 mm × 1.6 mm, a bandwidth of 4.89–6.85 GHz, and a peak gain of 6.5 dB.

Compared to these alternatives, the antenna proposed in this communication exhibits exceptional characteristics: compact size, UWB capability, and high gain, ensuring efficient coverage across operational bands.

4. RECONFIGURABLE ANTENNA

In the envisioned antenna design, PIN diodes are employed for reconfiguration purposes owing to their compact dimensions and swift switching capabilities. This is attributed to their ability to modify the electrical length of both the radiator and ground plane, enabling the desired current flow based on the diode's state. To integrate the PIN diode, into the recommended antenna structure, we incorporate lumped resistance-inductor-capacitor (RLC) components.

To enable electronic reconfiguration in the proposed design, we created an equivalent circuit model for PIN diodes, as visualized in Fig. 9 and its datasheet [37]. In the "ON" state, a low-value resistor is in series with a 0.15 nH inductance to facilitate current flow.

As a result, the electrical length of the radiator and ground plane increases, connecting the conducting portions of the antenna, as shown in Fig. 9(a). Conversely, in Fig. 9(b) the reverse state is depicted where a high-value resistor (7 kΩ) is connected in parallel with a 0.017 pF capacitor, and this combination is then placed in series with a 0.15 nH inductor. The elevated resistance and capacitance values prevent current flow in the reverse bias condition, accounting for the diode's blocked state. The circuit comprises a direct current (DC) source, with two voltage settings: 3 V in the forward direction and 0 V in the reverse direction. This source is linked in series with a 1 K-ohm resistor to regulate the current flow. Subsequently, it is also connected in series with a 68 nH inductor designed to impede the alternating current [38]. This leads to a frequency range spanning from 3 GHz to 14 GHz.

Utilizing Ansoft HFSS to simulate PIN diodes offers versatility in terms of adapting to various resonance frequency bands. Two diodes are positioned within the antenna setup, situated between the parasitic elements and the main patch of the antenna, as illustrated in Fig. 10. These diodes serve as integral components, actively shaping and controlling signal characteristics for efficient transmission and reception. This arrangement highlights the pivotal role of diodes in optimizing the antenna system's overall performance, making it well suited for diverse application.

In Table 3, the states and positions representing different configurations of the PIN diodes are categorized. The electrical length of the antenna is determined by the ON/OFF states of the switch. In this table, '0' signifies the OFF state, while '1' signifies the ON state. Four modes are discussed, encompassing a voltage standing wave ratio (VSWR) within the 1–2 range, a wide bandwidth, reasonable gain, and exceptional radiation efficiency across all operational frequencies.

Figure 11 illustrates the simulated and measured reflection coefficients across four distinct operating modes: (a) Mode I; (b) Mode II; (c) Mode III; and (d) Mode IV.

Figure 12 presents a comprehensive view of the simulated reconfigurable antenna's performance across four distinct switching modes, offering valuable insights into its functionality and effectiveness. The three subplots within Fig. 12(a) peak gain, (b) radiation efficiency, and (c) VSWR provide critical data points that are essential for assessing the antenna's capabilities. (a) peak gain showcases its maximum gain in different configurations. The radiation efficiency, found in (b), reveals how efficiently the antenna converts input power into radiated energy, and (c) VSWR gives insights into its voltage standing wave ratio, indicating how well the antenna impedance matches that of the transmission line. In terms of impedance matching, the VSWR consistently remains between 1 and 2 throughout the entire operational bandwidth, ensuring efficient energy transfer and peak performance for all modes. This comprehensive

TABLE 3. Various pin diode configurations and their respective operating frequency ranges.

Mode	Diodes		Frequency band GHz	Resonance frequency (GHz)	Peak gain (dB)	Radiation efficiency %
	D1	D2				
I	0	0	3.9–10.3, 10.88–14	4.66/7.71/9.81/12.69	2.4 to 7.1	0.8–0.98, 0.89–0.98
II	0	1	3.26–4.22, 5.27–14	3.61/5.79/9.37/10.68/12.25	1.7 to 6.57	0.80–0.89, 0.75–0.96
III	1	1	3–4.22, 8.66–9.76, 10.71–13.85	3.53/9.32/12.77	1.57 to 8.3	0.89–0.92, 0.76–0.88, 0.87–0.97
IV	1	0	3.21–4.31, 5.36–10.24, 11.03–13.91	3.70/5.97/9.72/12.86	1.7 to 5.36	0.80–0.90, 0.73–0.94, 0.87–0.95

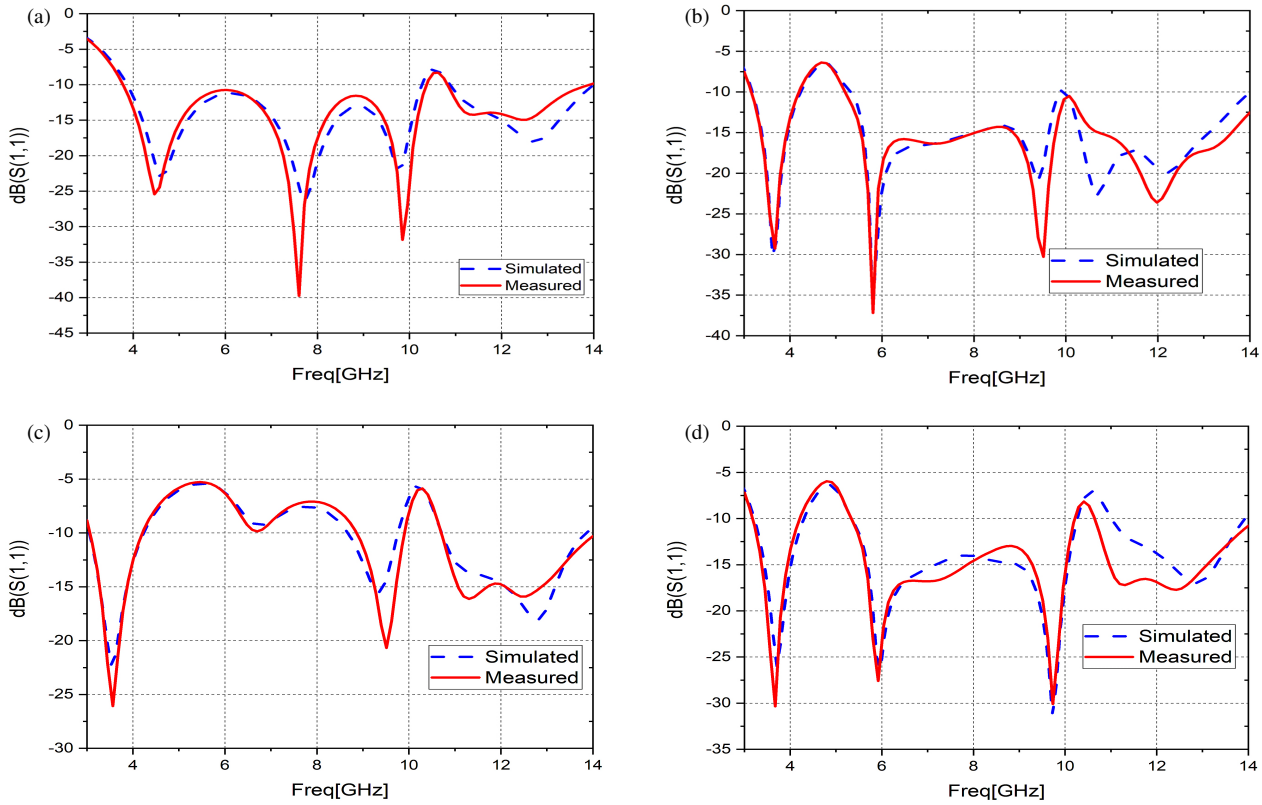

FIGURE 11. Simulated and measured S_{11} at the four operating modes: (a) Mode I; (b) Mode II; (c) Mode III; and (d) Mode IV.

visualization serves as a vital resource for understanding the antenna's performance under varying conditions.

4.1. Mode I: D1 D2 OFF

Figure 11 shows the simulated and measured S_{11} characteristics for mode 1 of the antenna, with all switches in the OFF position. This mode reveals that the antenna behavior across a broad frequency range, spanning 3.9–10.3 GHz and 10.88–14 GHz, with notable resonances occurring at 4.66, 7.71, 9.81, and 12.69 GHz, is accompanied by varying peak gains, ranging from 2.4 to 7.1 dB, making the antenna adaptable to different signal strength and clarity requirements. Furthermore, the antenna's radiation efficiency varies from 0.8% to 0.98% across the frequency bands, demonstrating its capability to perform optimally under diverse conditions. This comprehensive analysis underscores the antenna's versatility and suitability for a wide range of communication and signal-processing applications. A wideband antenna operating from 3.9 to 10.3 GHz, and 10.88 to 14 GHz covers a broad range of frequencies, making it versatile for various applications. In the lower part of this frequency range (3.9 GHz to 6 GHz), the antenna can be employed for terrestrial and satellite communication systems. It is well

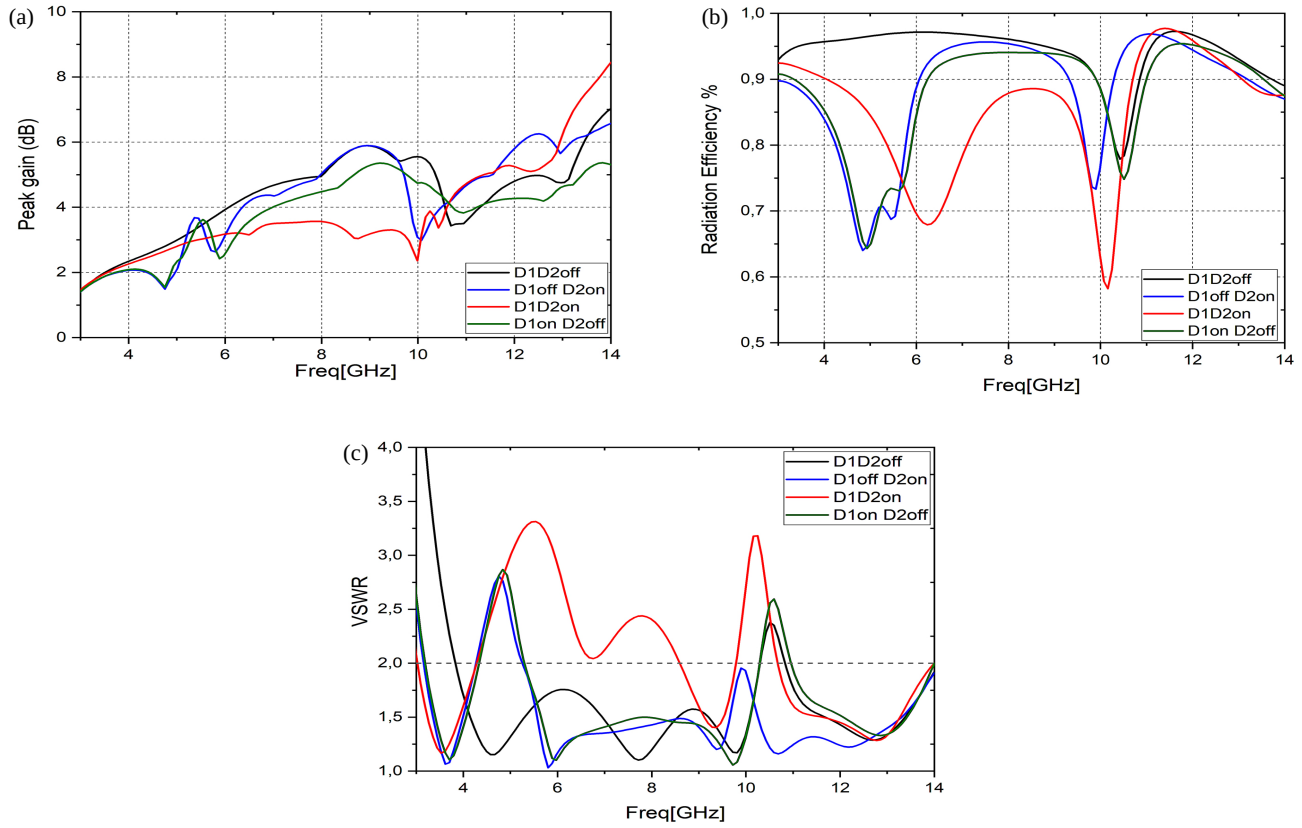

FIGURE 12. Simulated antenna performance in four switching modes: (a) peak gain; (b) radiation efficiency; (c) VSWR.

suited for Wi-Fi, WiMAX, and point-to-point microwave links, enabling high-speed data transmission and long-distance connectivity. Moving into the higher frequency range (6 GHz to 14 GHz), the antenna finds use in radar applications, both military and civilian, which includes weather radar, air traffic control radar, and automotive radar for collision avoidance. With its wide frequency coverage, this antenna is a valuable tool for a range of modern communication and sensing systems.

4.2. Mode II: D1OFF D2ON

The improved mode of the reconfigurable antenna presents a dual-band performance, covering the frequency ranges of 3.26–4.22 GHz and 5.27–14 GHz. Within these bands, the antenna exhibits notable resonances at specific frequencies: 3.61 GHz, 5.79 GHz, 9.37 GHz, 10.68 GHz, and 12.25 GHz. Furthermore, the antenna demonstrates radiation efficiency ranging from 0.80% to 0.89% in the lower band and 0.75% to 0.96% in the higher band. The peak gain of this reconfigurable antenna varies across its operating range, with values ranging from 1.7 dB to 6.57 dB. Such characteristics make this antenna well suited for a variety of applications, including telecommunications, radar systems, and wireless communication, where dual-band operation and high selectivity are crucial for optimal performance.

An antenna designed to operate in the 3.26–4.22 GHz and 5.27–14 GHz frequency ranges finds applications across a spectrum of modern technology. The lower frequency range, 3.26–4.22 GHz, is well suited for everyday wireless connectivity, including Wi-Fi and Bluetooth, providing the backbone for seamless internet access and device communication. Meanwhile, the broader span of 5.27–14 GHz sees utilization in more advanced systems, such as X-band radar for weather monitoring and military applications, Ku-band satellite communication for global data transmission, and point-to-point microwave links ensuring high-capacity, long-distance data exchange.

4.3. Mode III: D1 D2 ON

The enhanced configuration of the reconfigurable antenna of this mode offers a tri-band performance, encompassing frequency bands from 3 to 4.22 GHz, 8.66 to 9.76 GHz, and 10.71 to 13.85 GHz. This antenna operates at resonant frequencies of 3.53, 9.32, and 12.77 GHz, delivering a peak gain that varies from 1.57 to 8.3 dB and radiation efficiency ranging from 0.76% to 0.97% within its operating bands.

In the lower frequency band of 3 to 4.22 GHz, the antenna aligns with applications such as Wi-Fi and Bluetooth, enabling wireless connectivity and communication in homes, offices, and public spaces. Meanwhile, in the higher bands, it serves in more advanced roles, including X-band radar for weather monitoring, Ku-band satellite communication for global data transmission, and point-to-point microwave links, ensuring high-capacity, long-distance data exchange. This wide frequency coverage showcases the antenna's versatility, spanning from everyday connectivity to critical radar and satellite communication systems.

TABLE 4. Performance comparison of the proposed reconfigurable UWB antenna and some existing designs in the literature.

Ref.	Type of substrate	Size (mm^2)	Cover band (GHz)	No diode
[25]	FR4	36×34	2.8–10.3	2
[26]	FR4	25×21	3.1–10	2
[27]	FR4	42×32	2.7–14.9	1
[28]	Rogers RO5870	50×50	1–10	2
[29]	FR4	36×46	3–11	4
[30]	ROJERS	35×24	2.8–13	3
[31]	FR4	30×30	2–12	2
[32]	FR4	30×35.5	3.53–9.56	3
[33]	FR4	40×60	2–10	3
[34]	Rogers 5880	35×55	2.8–11	2
[38]	ROGERS TMM4	17×23	2.8–10.6	2
[39]	FR4	52×59	1.82–3.61 5.24–12.43	4
Proposed antenna	FR4	30×22	3–14	2

4.4. Mode IV: D1ON D2OFF

The upgraded design of this reconfigurable antenna mode provides triple-band performance across frequency ranges spanning from 3.21 to 4.31 GHz, 5.36 to 10.24 GHz, and 11.03 to 13.91 GHz. Functioning at resonant frequencies of 3.70, 5.97, 9.72, and 12.86 GHz, the antenna yields a peak gain ranging from 1.7 to 5.36 dB, coupled with radiation efficiency ranging from 0.73% to 0.95% within its operational bands.

The novel antenna was assessed against recent models, highlighting its uniqueness. Table 4 summarizes the comparison, revealing its advantages in terms of increased passbands, flexibility, cost-effectiveness, and a more compact size. The findings underscore the superior performance of the recommended antenna in various aspects.

5. CONCLUSION

This paper presents an innovative design for a fractal reconfigurable ultra-wideband (UWB) antenna. The antenna incorporates two plus-shaped parasitic elements and a hexagonal radiating patch while maintaining a compact size of 30 mm × 22 mm × 1.6 mm, thanks to the cost-effective FR4 substrate. A partial ground plane with an integrated rectangular slot enhances performance. The design was meticulously developed using HFSS, and the fabricated prototype demonstrated excellent agreement between measured and simulated results. A key distinguishing feature of this antenna is the integration of two strategically placed PIN diodes, enabling precise control over current distribution and tunable resonant frequencies through various switch combinations. This reconfigurability significantly extends the operating bands from 3 to 14 GHz, enhancing frequency coverage and overall antenna performance. Additionally, its compact dimensions make it an attractive option for manufacturers' integrating multiple antennas into small electronic devices without design complications. This enhanced design represents a significant advancement in UWB antennas, offering both versatility and high performance for modern wireless communication applications.

ACKNOWLEDGEMENT

The authors would like to thank Universiti Teknikal Malaysia Melaka (UTeM), the Ministry of Higher Education (MOHE) of Malaysia, and Sultan Moulay Slimane University, Morocco for supporting this project.

REFERENCES

[1] Ghadeer, S. H., S. K. A. Rahim, M. Alibakhshikenari, B. S. Virdee, T. A. Elwi, A. Iqbal, and M. Al-Hasan, "An innovative fractal monopole MIMO antenna for modern 5G applications," *AEU — International Journal of Electronics and Communications*, Vol. 159, 154480, 2023.

[2] Das, S., D. Mitra, and S. R. B. Chaudhuri, "Fractal loaded planar super wide band four element MIMO antenna for THz applications," *Nano Communication Networks*, Vol. 30, 100374, 2021.

[3] Elabd, R. H. and A. J. A. Al-Gburi, "Design and optimization of a circular ring-shaped UWB fractal antenna for wireless multiband applications using particle swarm optimization," *Progress In Electromagnetics Research B*, Vol. 106, 101–112, 2024.

[4] Benkhadda, O., M. Saih, A. Reha, S. Ahmad, K. Chaji, H. Singh, and A. J. A. Al-Gburi, "A miniaturized reconfigurable antenna for modern wireless applications with broadband and multi-band capabilities," *Progress In Electromagnetics Research M*, Vol. 127, 93–101, 2024.

[5] Marzouk, M., Y. Rhazi, I. H. Nejdi, F.-E. Zerrad, M. Saih, S. Ahmad, A. Ghaffar, and M. Hussein, "Ultra-wideband compact fractal antenna for WiMAX, WLAN, C and X band applications," *Sensors*, Vol. 23, No. 9, 4254, 2023.

[6] Marzouk, M., I. H. Nejdi, Y. Rhazi, and M. Saih, "Multiband and wide band octagonal fractal antenna for telecommunication applications," in *2022 8th International Conference on Optimiza-*

tion and Applications (ICOA), 1–6, Genoa, Italy, Oct. 2022.

[7] Kumar, A., G. Singh, M. K. Abdulhameed, S. R. Hashim, and A. J. A. Al-Gburi, "Development of fractal 5G MIMO antenna for sub 6 GHz wireless automotive applications," *Progress In Electromagnetics Research M*, Vol. 130, 121–128, 2024.

[8] Megahed, A. A., A. H. Hussein, A. J. A. Al-Gburi, and R. H. Elabd, "Compact wideband antenna array with DGS-based metamaterial for efficient smartphone communication and SAR reduction," *Progress In Electromagnetics Research B*, Vol. 110, 15–28, 2025.

[9] El Aoud, S. E., H. Abbaoui, O. Benkhadda, S. Attioui, N. E. Assri, S. Ibnyaich, A. Zeroual, M. M. Ismail, and A. J. A. Al-Gburi, "Design of a crescent moon-shaped reconfigurable patch antenna using a PIN diode for 5G sub-6 GHz and multistandard wireless applications," *Progress In Electromagnetics Research B*, Vol. 109, 81–93, 2024.

[10] Singh, A. K., S. K. Mahto, R. Sinha, M. Alibakhshikenari, A. J. A. Al-Gburi, A. Ahmad, L. Kouhalvandi, B. S. Virdee, and M. Dalarsson, "Low-loss paper-substrate triple-band-frequency reconfigurable microstrip antenna for sub-7 GHz applications," *Sensors*, Vol. 23, No. 21, 8996, 2023.

[11] Reha, A., O. Benkhadda, A. O. Said, A. E. Amri, and A. J. A. Al-Gburi, "Design of sub-6 GHz and sub-7 GHz dragon fractal antenna for 5G applications with enhanced bandwidth," *International Journal of Intelligent Engineering & Systems*, Vol. 18, No. 2, 14–22, 2025.

[12] Ibrahim, I. M., A. J. A. Al-Gburi, Z. Zakaria, and H. A. Bakar, "Parametric study of modified U-shaped split ring resonator structure dimension at ultra-wide-band monopole antenna," *Journal of Telecommunication, Electronic and Computer Engineering (JTEC)*, Vol. 10, No. 2–5, 53–57, 2018.

[13] Al-Gburi, A. J. A., I. Ibrahim, Z. Zakaria, and A. D. Khaleel, "Bandwidth and gain enhancement of ultra-wideband monopole antenna using MEBG structure," *ARPN Journal of Engineering and Applied Sciences (JEAS)*, Vol. 14, No. 10, 3390–3393, 2019.

[14] Addepalli, T., M. S. Kumar, C. R. Jetti, N. K. Gollamudi, B. K. Kumar, and J. Kulkarni, "Fractal loaded, novel, and compact two-and eight-element high diversity MIMO antenna for 5G sub-6 GHz (N77/N78 and N79) and WLAN applications, verified with TCM analysis," *Electronics*, Vol. 12, No. 4, 952, 2023.

[15] Al-Gburi, A. J. A., I. Ibrahim, and Z. Zakaria, "Band-notch effect of U-shaped split ring resonator structure at ultra wideband monopole antenna," *International Journal of Applied Engineering Research*, Vol. 12, No. 15, 4782–4789, 2017.

[16] Iqbal, J., U. Illahi, M. N. M. Yasin, M. A. Albreem, and M. F. Akbar, "Bandwidth enhancement by using parasitic patch on dielectric resonator antenna for sub-6 GHz 5G NR bands application," *Alexandria Engineering Journal*, Vol. 61, No. 6, 5021–5032, 2022.

[17] Paul, L. C., S. A. Hye, T. Rani, M. I. Hossain, M. Karaaslan, P. Ghosh, and H. K. Saha, "A compact wrench-shaped patch antenna with a slotted parasitic element and semi-circular ground plane for 5G communication," *E-Prime — Advances in Electrical Engineering, Electronics and Energy*, Vol. 6, 100334, 2023.

[18] Al-Gburi, A. J. A., I. B. M. Ibrahim, Z. Zakaria, and N. F. B. M. Nazli, "Wideband microstrip patch antenna for sub 6 GHz and 5G applications," *Przegląd Elektrotechniczny*, Vol. 97, No. 11, 26–29, 2021.

[19] Khan, I., K. Zhang, Q. Wu, I. Ullah, L. Ali, H. Ullah, and S. U. Rahman, "A wideband high-isolation microstrip MIMO circularly-polarized antenna based on parasitic elements," *Materials*, Vol. 16, No. 1, 103, 2023.

[20] Mojarrad, S. and y. zehforoosh, "Fractal multi input multi output antenna for WLAN applications," *Journal of Artificial Intelligence in Electrical Engineering*, Vol. 8, No. 30, 51, 2019.

[21] Al Gburi, A. J. A., "5G MIMO antenna: Compact design at 28/38 GHz with metamaterial and SAR analysis for mobile phones," *Przegląd Elektrotechniczny*, Vol. 100, No. 4, 171–174, 2024.

[22] Gençoğlan, D. N., "ANFIS-SA-based design of a hybrid reconfigurable antenna for L-band, C-band, 5G and ISM band applications," *Computers and Electrical Engineering*, Vol. 123, 110054, 2025.

[23] Tathare, S. S. and P. Goswami, "Design and development of a reconfigurable antenna with varactor diodes for next-generation wireless communication systems," *Computers and Electrical Engineering*, Vol. 123, 110091, 2025.

[24] Ma, S., W. Yang, J. Li, Q. Xue, and W. Che, "Millimeter-wave reconfigurable antenna based on VO_2 ink achieved by a simple process," *Materials & Design*, Vol. 250, 113583, 2025.

[25] Rahman, S. U., Q. Cao, Y. Li, I. Gil, and W. Yi, "Design of tri-notched UWB antenna based on elliptical and circular ring resonators," *International Journal of RF and Microwave Computer-Aided Engineering*, Vol. 29, No. 3, e21648, 2019.

[26] Nazeri, A. H., A. Falahati, and R. M. Edwards, "A novel compact fractal UWB antenna with triple reconfigurable notch reject bands applications," *AEU — International Journal of Electronics and Communications*, Vol. 101, 1–8, 2019.

[27] Lakrit, S., S. Das, A. E. Alami, D. Barad, and S. Mohapatra, "A compact UWB monopole patch antenna with reconfigurable Band-notched characteristics for Wi-MAX and WLAN applications," *AEU — International Journal of Electronics and Communications*, Vol. 105, 106–115, 2019.

[28] Belkadi, B., Z. Mahdjoub, M. L. Seddiki, and M. Nedil, "UWB monopole antenna with reconfigurable notch bands based on metamaterials resonators," in *2018 IEEE International Symposium on Antennas and Propagation & USNC/URSI National Radio Science Meeting*, 285–286, Boston, MA, USA, Jul. 2018.

[29] Yadav, A., G. Kumar, and R. P. Yadav, "Frequency reconfigurable dual notch UWB antenna," in *2020 International Conference on Wireless Communications Signal Processing and Networking (WiSPNET)*, 1–6, Chennai, India, Aug. 2020.

[30] Li, J. and Y. Sun, "Reconfigurable triple band-notched monopole UWB antenna," in *2019 Cross Strait Quad-Regional Radio Science and Wireless Technology Conference (CSQRWC)*, 1–3, Taiyuan, China, Jul. 2019.

[31] Ud Din, I., S. Ullah, K. Ullah, Y. Fawad, I. Ahmad, S. Ullah, and U. Habib, "Circular monopole ultra-wideband (UWB) antenna with reconfigurable band-notched characteristics," in *2020 IEEE 23rd International Multitopic Conference (INMIC)*, 1–6, Bahawalpur, Pakistan, Nov. 2020.

[32] Wang, S., J. Dong, and M. Wang, "A frequency-reconfigurable UWB antenna with switchable single/dual/triple band notch functions," in *2019 Cross Strait Quad-Regional Radio Science and Wireless Technology Conference (CSQRWC)*, 1–3, Taiyuan, China, Jul. 2019.

[33] Khan, T., M. Rahman, A. Akram, Y. Amin, and H. Tenhunen, "A low-cost CPW-fed multiband frequency reconfigurable antenna for wireless applications," *Electronics*, Vol. 8, No. 8, 900, 2019.

[34] Hui, Y., H. Zu, R. Song, H. Fu, K. Luo, C. Tian, B. Wu, G.-L. Huang, Z. Kou, X. Cheng, and D. He, "Graphene-assembled film-based reconfigurable filtering antenna with enhanced corrosion-resistance," *Crystals*, Vol. 13, No. 5, 747, 2023.

[35] Benkhadda, O., M. Saih, S. Ahmad, A. J. A. Al-Gburi, Z. Zakaria, K. Chaji, and A. Reha, "A miniaturized tri-wideband Sierpinski hexagonal-shaped fractal antenna for wireless communication applications," *Fractal and Fractional*, Vol. 7, No. 2, 115, 2023.

[36] Varshney, A., N. Cholake, and V. Sharma, "Low-cost ELC-UWB fan-shaped antenna using parasitic SRR triplet for ISM band and PCS applications," *International Journal of Electronics Letters*, Vol. 10, No. 4, 391–402, 2022.

[37] https://4donline.ihs.com/images/VipMasterIC/IC/AVGO/AVGOS00610/AVGOS00610-1.pdf?hkey=6D3A4C79FDBF58556-ACFDE234799DDF0 n.d.

[38] Zaidi, A., W. A. Awan, A. Ghaffar, M. S. Alzaidi, M. Alsharef, D. H. Elkamchouchi, S. S. M. Ghoneim, and T. E. A. Alharbi, "A low profile ultra-wideband antenna with reconfigurable notch band characteristics for smart electronic systems," *Micromachines*, Vol. 13, No. 11, 1803, 2022.

[39] Varshney, A., T. M. Neebha, V. Sharma, J. G. Jency, and A. D. Andrushia, "Dodecagon-shaped frequency reconfigurable antenna practically loaded with 3-delta structures for ISM band and wireless applications," *IETE Journal of Research*, Vol. 69, No. 11, 7747–7759, 2023.